

Direct VLBI Detection of Interstellar Turbulence Imprint on a Quasar: TXS 2005+403

A. V. PLAVIN ¹, A. B. PUSHKAREV ² AND Y. Y. KOVALEV ³

¹*Black Hole Initiative, Harvard University, 20 Garden St, Cambridge, MA 02138, USA*

²*Crimean Astrophysical Observatory, 298409 Nauchny, Crimea*

³*Max-Planck-Institut für Radioastronomie, Auf dem Hügel 69, Bonn D-53121, Germany*

(Received February 27, 2026)

ABSTRACT

We report the first unambiguous detection of refractive substructure in an active galactic nucleus (AGN) using ground-based Very Long Baseline Interferometry (VLBI). Our analysis of TXS 2005+403 — observed at 1–5 GHz along a line of sight through the Cygnus region — reveals clear signatures of turbulence-induced substructure on long baselines that cannot be explained by the smooth scatter-broadened profile from diffractive effects alone. This signal persists across multiple observations spanning 2010–2019, demonstrating stable scattering properties along the line of sight. The combination of high flux density, compact intrinsic structure, and strong scattering establishes TXS 2005+403 as an exceptional laboratory for probing Galactic turbulence. This detection demonstrates that AGNs can serve as cosmic lighthouses illuminating interstellar plasma across the sky, complementing pulsar scintillation studies and informing scattering mitigation for millimeter-wavelength imaging of Sagittarius A*.

Keywords: Interstellar scattering (854) — Very long baseline interferometry (1769) — Active galactic nuclei (16) — Blazars (164) — Interstellar medium (847)

1. INTRODUCTION

Extremely compact radio sources, such as active galactic nuclei (AGNs) with milliarcsecond (mas)-scale emission, are affected by scattering in the ionized interstellar medium of the Milky Way. Electron density fluctuations along the line of sight act as a turbulent “screen” that distorts the incoming radio waves. Diffractive scattering blurs compact sources into smooth, broadened profiles (P. J. Duffett-Smith & A. C. S. Readhead 1976; B. J. Rickett 1990), while refractive scattering from turbulent density fluctuations imprints additional small-scale substructure (R. Narayan & J. Goodman 1989; M. D. Johnson & C. R. Gwinn 2015; M. D. Johnson & R. Narayan 2016; M. D. Johnson 2016).

Radio Very Long Baseline Interferometry (VLBI), which achieves the highest angular resolution in astronomy by combining signals from telescopes separated by thousands of kilometers, is ideally suited to studying both effects. We previously measured diffractive broad-

ening in large samples of AGNs and constructed all-sky scattering maps (A. B. Pushkarev & Y. Y. Kovalev 2015; T. A. Koryukova et al. 2022). Refractive substructure is far more challenging to detect. Substructure within scatter-broadened images was first observed in RadioAstron space VLBI studies of heavily scattered pulsars (C. R. Gwinn et al. 2016; M. V. Popov et al. 2017, 2020). In the context of compact continuum sources, it was detected for Sagittarius A* at 1.3 cm using the VLBA together with the Green Bank Telescope and interpreted as refraction by large-scale plasma fluctuations (C. R. Gwinn et al. 2014), with subsequent observations and modeling (M. D. Johnson et al. 2018; S. Issaoun et al. 2019; M. D. Johnson et al. 2021). For AGNs, RadioAstron has provided detections consistent with refractive substructure in 3C 273 (M. D. Johnson et al. 2016) and B 0529+483 (S. V. Pilipenko et al. 2018), but the interpretation is complicated by the degeneracy with intrinsic compact structure. AGNs provide background sightlines that sample the full Galactic column, unlike pulsars, which are nearby and concentrated toward the Galactic plane. Exploiting refractive scattering as a probe of the interstellar medium requires bright, heavily scat-

tered AGNs, for which compact substructure is both detectable and not degenerate with the intrinsic emission.

One such source is the blazar TXS 2005+403 ($z = 1.736$; [A. Boksenberg et al. 1976](#)), a bright (about 2 Jy) source behind the Cygnus region, where plasma clouds produce strong Galactic scattering ([T. A. Koryukova et al. 2022](#)). At frequencies $\gtrsim 15$ GHz, where scattering is subdominant, it displays a typical one-sided parsec-scale jet with superluminal apparent motion ([T. A. Koryukova et al. 2023](#); [M. L. Lister et al. 2021](#)). At lower gigahertz frequencies, scattering along this line of sight was recently quantified through diffractive broadening measured with VLBI and through extreme scattering events in single-dish light curves ([T. A. Koryukova et al. 2023, 2025](#)); it was further discussed in [L. Y. Petrov & Y. Y. Kovalev \(2025\)](#) as a limiting factor for astrometric accuracy. The combination of high flux density and strong scattering makes TXS 2005+403 particularly well suited for probing interstellar plasma properties with VLBI.

Here, we report the first direct detection of refractive scattering substructure in an AGN using ground-based VLBI. We analyze archival Very Long Baseline Array (VLBA) observations of TXS 2005+403 at 1–5 GHz spanning nearly a decade (Section 2), characterize anisotropic diffractive broadening (Section 3.1), and detect refractive substructure manifested as an otherwise unexplained long-baseline visibility signal (Section 3.2). The detected signal is consistent with interstellar turbulence models (Section 3.3). We summarize and discuss future prospects in Section 4.

2. DATA

Our analysis focuses on 1–5 GHz, where refractive and diffractive scattering effects from the interstellar medium are most pronounced. We use Very Long Baseline Array (VLBA) observations from 2010–2019 available in the NRAO data archive, experiment codes BG196, BG246, BG258, BS224, and UG002. A summary of these observations is provided in [Table 1](#). The observations used 16–256 MHz total bandwidth (per feed polarization) split into 4–8 intermediate-frequency subbands (hereafter IFs), depending on the experiment. All datasets were calibrated using common *AIPS* ([E. W. Greisen 2003](#)) procedures for VLBI data reduction.

3. RESULTS

3.1. Anisotropic Diffractive Broadening

As demonstrated in [T. A. Koryukova et al. \(2023\)](#), the morphology of TXS 2005+403 is dominated by its parsec-scale jet at $\gtrsim 8$ GHz and by scatter broadening at $\lesssim 5$ GHz. Here, we focus on the latter frequency

Table 1. VLBA observations and long-baseline detections for TXS 2005+403.

Exp code (1)	Epoch (2)	Band (GHz) (3)	BW (MHz) (4)	Long-baseline detections	
				Per IF (5)	Combined (6)
BG196	2010-11-05	L (1.4–1.8)	64	286/5416 (5%)	274/2712 (10%)
BS224	2013-07-04	L (1.4–1.8)	16	10/28684 (0%)	136/3586 (4%)
BG246	2017-07-12 – – 2018-01-08	L (1.4–1.8)	256	2688/11052 (24%)	1503/2760 (54%)
		S (2.3)	256	874/6034 (14%)	379/746 (51%)
		C (5.0)	256	581/1186 (49%)	127/148 (86%)
UG002	2018-08-11	S (2.3)	128	52/241 (22%)	35/59 (59%)
BG258	2019-02-20	L (1.4–1.8)	256	795/3554 (22%)	499/888 (56%)
		S (2.3)	256	252/1860 (14%)	83/230 (36%)
		C (5.0)	256	178/178 (100%)	22/22 (100%)

NOTE—Columns are as follows: (1) – experiment code; (2) – observation epochs for the experiment as YYYY-MM-DD; (3) – frequency band name and its base frequency; (4) – total bandwidth (per polarization); (5) – detections from individual IF fringe searches (format: # detections/total tested); (6) – detections when adjacent IFs are combined. Long-baseline detections are defined as signal detected on baselines beyond where the diffractive-broadening Gaussian model reaches 1/1000 of its peak amplitude. Detection threshold is defined in [subsection 3.2](#).

range (1–5 GHz), corresponding to VLBA bands L, S, and C.

To characterize diffractive broadening, we fit a single elliptical Gaussian component to each frequency band in every experiment. We use only short baselines (where visibility SNR exceeds 10) and fit closure amplitudes to avoid relying on a priori calibration. The elliptical Gaussian model shows excellent agreement with the short-baseline data at 1–5 GHz ([Figure 1](#)). The fitted sizes ([Figure 2](#)) follow the $1/\nu^2$ scaling expected in the scattering-dominated regime ([B. J. Rickett 1990](#)). At 5 GHz, intrinsic source structure likely contributes, causing a slight size increase — particularly along the minor axis, where scattering is weaker. The minor axis also lies close to the inner jet direction ([A. V. Plavin et al. 2022](#); [T. A. Koryukova et al. 2023](#)), so we exclude the 5 GHz band from the power-law fit. The fit-

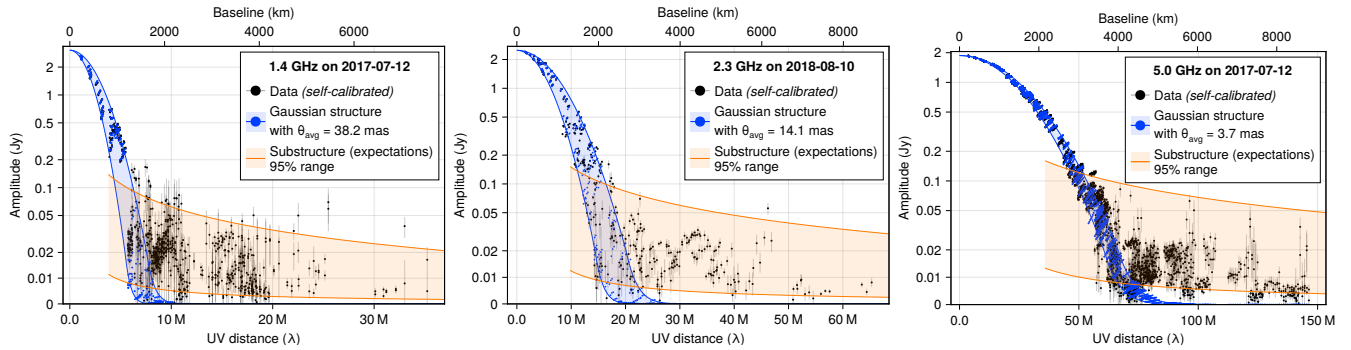


Figure 1. Visibility amplitude versus projected baseline length or uv -distance. Experiments with the best sensitivity and coverage are shown in each frequency band, left to right: L, S, C bands. Data (black points with 1σ error bars) are self-calibrated to per-IF elliptical Gaussian models (blue points). The blue shaded band shows the average Gaussian model within each band. The predicted refractive substructure signal is shown as the orange band starting from the uv -distance where the Gaussian model first falls to 25% of its peak. Its calculations assume scattering with broadening size equal to the average axis of the Gaussian (see subsection 3.3).

ted ellipse shape remains consistent across epochs and frequencies, with elongation aligned along the Galactic plane. This alignment was first reported for another blazar (B2 2023+335) in A. B. Pushkarev et al. (2013) and detected for TXS 2005+403 in T. A. Koryukova et al. (2023). Such elongation may indicate persistent structures in the plasma screen that are aligned perpendicular to the Galactic plane. In what follows, we use this understanding of diffractive broadening to robustly distinguish refractive substructure from potential intrinsic source structure.

3.2. Refractive Substructure Detection

The Gaussian models describe the large-scale source structure well. However, as shown in Figure 1, we observe significant signal on long baselines well beyond where the Gaussian envelope predicts any measurable flux. This excess cannot arise from intrinsic blazar structure: interstellar scattering acts as a convolution, so the observed visibility is the product of the intrinsic visibility and the Fourier transform of the scattering kernel. At baselines where this kernel — well described by a Gaussian (subsection 3.1) — drops below 10^{-3} of its peak, any intrinsic emission is multiplicatively suppressed to negligible levels regardless of its morphology. This leaves refractive substructure from turbulence in the interstellar medium as the only mechanism capable of producing correlated signal beyond the broadening envelope (see Figure 4 for an illustration). The strong scattering toward TXS 2005+403 creates a clean separation in the uv plane: diffractive broadening dominates on short baselines, while only refractive substructure contributes on long baselines — a regime distinction not accessible for the AGNs studied earlier.

The data in Figure 1 are obtained from *AIPS* processing with antenna-based fringe fitting performed indepen-

dently for each IF. We require a baseline signal-to-noise ratio (SNR) cutoff of 5 and a minimum of three antennas for a detection. We then self-calibrate them (both amplitude and phase of the gains; no temporal correlation enforced) to the per-IF Gaussian models from subsection 3.1. As shown, *AIPS* yields numerous detections on baselines longer than expected from the Gaussian structure.

These visibilities exceed the commonly used SNR threshold, but only by a factor of a few. Since *AIPS* SNR estimates can be biased (see discussion in L. Petrov et al. 2011; Y. Y. Kovalev et al. 2020; T. Savolainen et al. 2023), we implement an independent baseline-based fringe search on the raw correlator data from the VLBA archive to ensure the reliability of the long-baseline signal detections. We compute the Fast Fourier Transform (FFT) of each scan and IF without restricting the search window. This search yields a $\pm 1 \mu\text{s}$ delay range (defined by the spectral-channel spacing within each IF) and a $\pm 0.1\text{--}0.3$ Hz rate range (depending on the correlator integration time). As expected, individual FFT amplitudes follow Gaussian statistics in scans without any detected signal. All FFT output values are independent for a pure noise input without oversampling, and the spurious detection probability is $\mathbb{P}(\text{peak}|\text{noise}) \leq N e^{-\text{SNR}^2/2}$, where N is the number of search grid cells (L. Petrov et al. 2011). We use $2\times$ oversampling in delay and rate to reduce peak amplitude loss from $\times 2.5$ to $\times 1.2$ (L. Petrov et al. 2011). Oversampling introduces dependencies between FFT values, so the output contains fewer than N independent values. We conservatively retain the same probability formula, which becomes an upper bound. We adopt $\mathbb{P}(\text{peak}|\text{noise}) < 5 \times 10^{-5}$ as the conservative detection threshold, corresponding to fewer than 0.5 expected spurious detections across all observa-

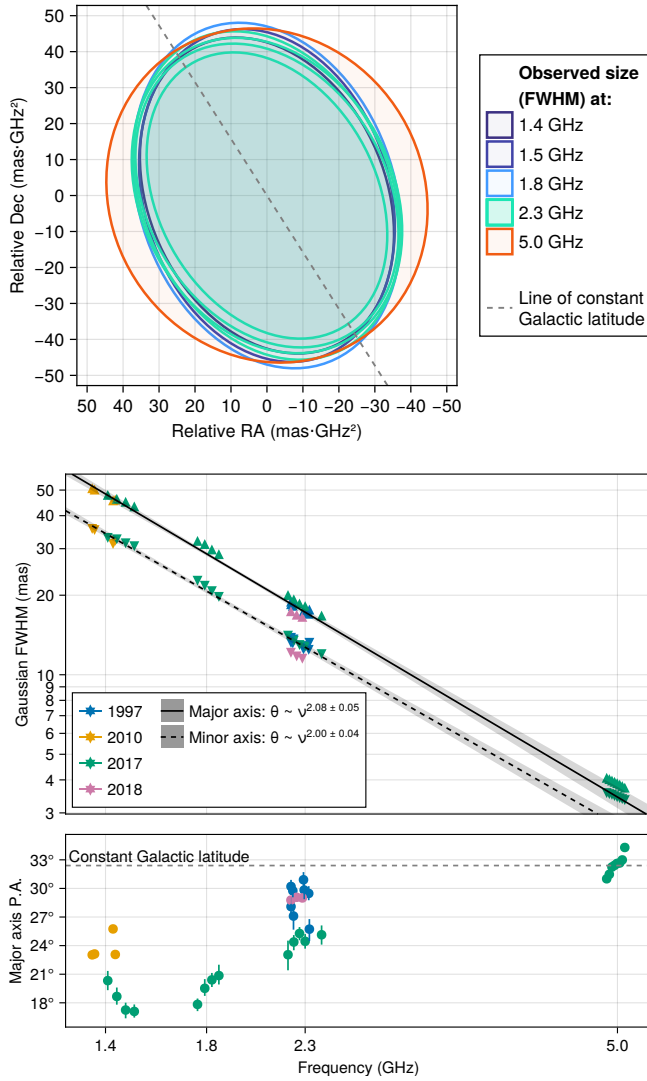


Figure 2. Elliptical Gaussian fits to VLBA observations at 1–5 GHz.

Top: Gaussian contours at the half-maximum level (FWHM) in RA–Dec space; each ellipse represents a single observation, with sizes normalized by ν^{-2} for direct comparison across frequencies.

Middle and bottom: Frequency dependence of Gaussian major and minor axes (middle) and position angle (bottom); each point represents a single IF with 2σ uncertainties shown. All panels show clear ν^{-2} size scaling and consistent elongation along the Galactic plane.

tions. We first search each IF individually, then combine adjacent IFs to increase bandwidth and sensitivity.

A summary of long-baseline signal detections is given in Table 1 and shown in Figure 3. We find numerous detections even when treating individual IFs separately; the SNR and detection fraction increase further when adjacent IFs are combined. This is qualitatively consistent with the *AIPS* fringe search: a long-baseline signal incompatible with pure diffractive broadening is clearly

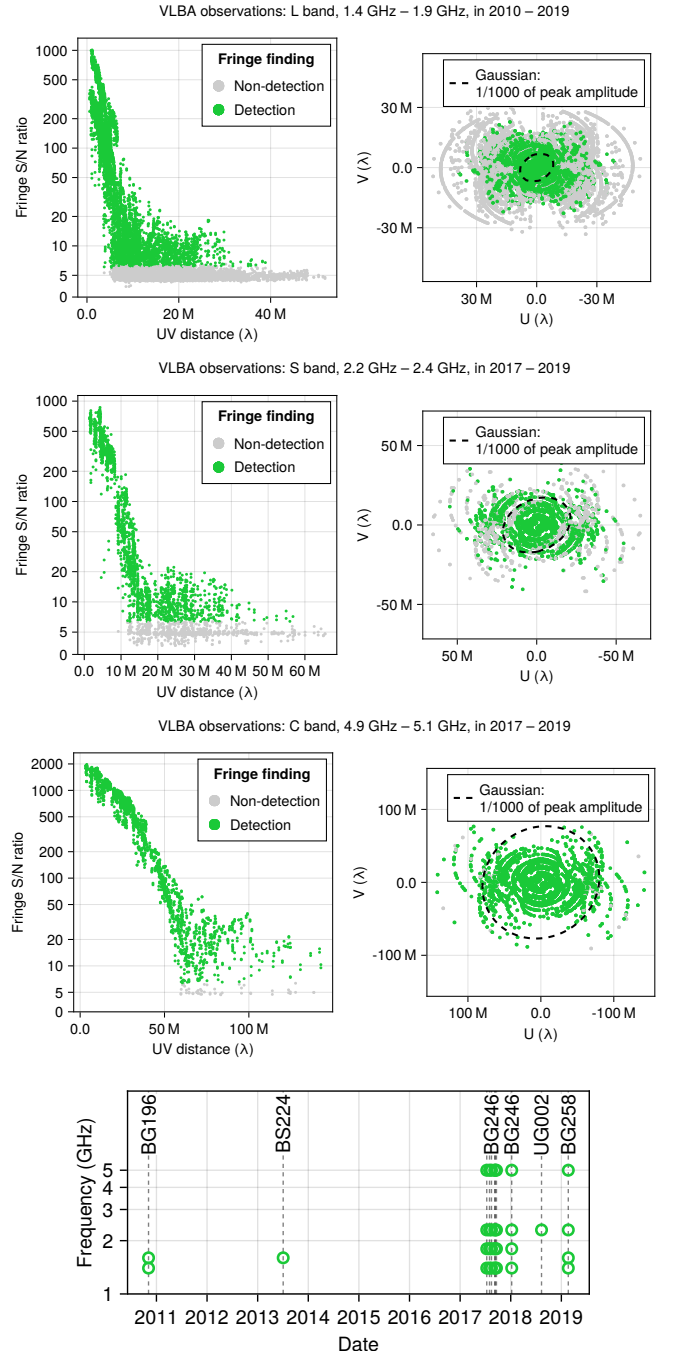


Figure 3. Long-baseline detections in VLBA observations of TXS 2005+403 over 2010–2019.

Top: Individual panels show detections at 1, 2, and 5 GHz when adjacent IFs are combined, displaying their SNR and uv -plane locations. Elliptical contours in the uv plane mark where the diffractive-broadening Gaussian reaches 1/1000 of its peak — a conservative boundary beyond which no signal is expected from pure scatter broadening. See subsection 3.2 and Table 1 for detection details and threshold definitions.

Bottom: Times and frequencies of all observations with detected long-baseline signal. Coverage spanning about a decade indicates persistent refractive substructure in TXS 2005+403.

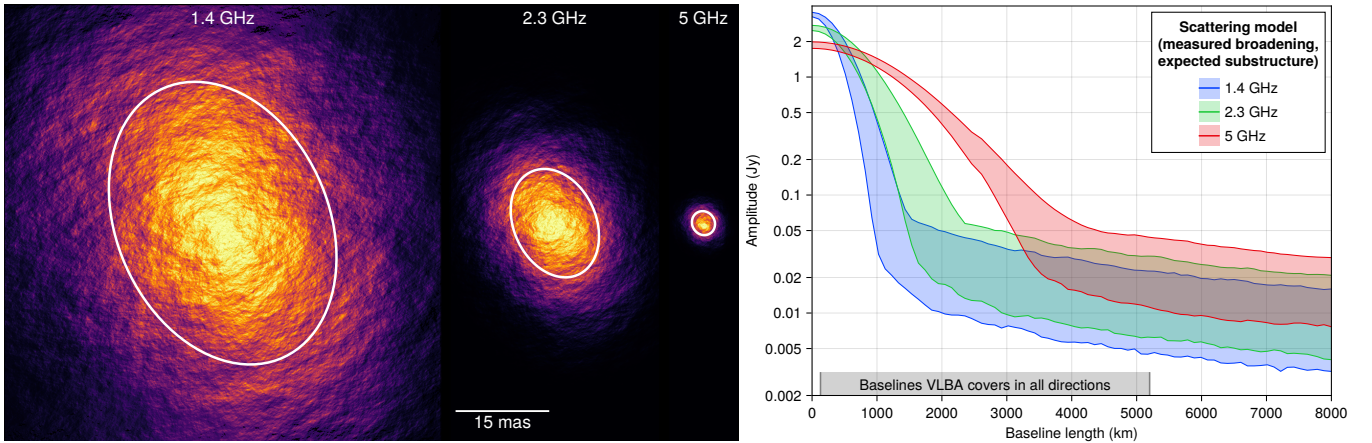


Figure 4. Simulated scattering of TXS 2005+403 using parameters consistent with our observations (subsection 3.3). *Left:* a single realization of the scattered image at 1.4, 2.3, and 5 GHz, showing both the large-scale Gaussian broadening and fine-scale refractive substructure from turbulent density fluctuations in the scattering screen. White ellipses mark the measured FWHM sizes from elliptical Gaussian fits (Figure 2), averaged per band. *Right:* visibility amplitude predictions; shaded bands show the 95% range across random screen realizations. The highlighted baseline range indicates where the VLBA provides good position angle coverage.

An interactive version of this figure is available at <https://github.com/aplavin/txs2005-refractive-substructure>.

present across all three frequency bands (1, 2, 5 GHz) over many years (2010–2019). We therefore conclude that refractive substructure in TXS 2005+403 has been detected using ground-based VLBI — for the first time in any AGN. The substructure effects persist over nearly a decade (Figure 3).

3.3. Comparison with Turbulence Models

Having detected the refractive scattering substructure, we now evaluate how its properties compare with model expectations. Here, we use the data that were a priori calibrated and fringe-fitted in *AIPS* (section 2). The substructure introduces a fundamentally stochastic signal in the visibilities. We compare the M. D. Johnson & C. R. Gwinn (2015) model to the observed long-baseline structure, computing expected visibility amplitude variations from a power-law turbulence scale spectrum with $\alpha = 5/3$, an inner scale $r_{\text{in}} = 1000$ km, and a screen distance $D = 1.4$ kpc (corresponding to the Cygnus region; K. L. J. Rygl et al. 2012). The observed data generally fall within the predicted range (Figure 1); Figure 4 shows simulated images with substructure based on these parameters. Given the limitations of the available data, especially the effective noise level, we perform only this consistency check and do not attempt to constrain the turbulent screen properties.

In principle, even diffractive broadening alone can constrain the inner turbulence scale r_{in} : on baselines longer than r_{in} , visibilities should deviate from the Gaussian profile. See M. D. Johnson et al. (2018) for discussion and derivation of a Kolmogorov turbulence spectrum. The sensitivity and baseline coverage in the exist-

ing data are insufficient to reliably distinguish Gaussian from non-Gaussian behavior. Still, with its strong scattering and high flux density, TXS 2005+403 is a prime candidate for probing these turbulence properties using both broadening and substructure observables. These two regimes are well-separated by baseline length for this line of sight at gigahertz frequencies, and are readily accessible to ground-based VLBI arrays. We plan to pursue this with our ongoing VLBA campaign, together with a more detailed substructure variability analysis.

The turbulent scattering models indicate that the 1–10 GHz VLBI regime is optimal for heavily scattered AGNs like TXS 2005+403: broadening dominates the apparent structure while refractive scattering produces measurable long-baseline correlated signal. The refractive visibility fluctuations are expected to be even larger at higher frequencies (see the right panel of Figure 4) on baselines accessible to space VLBI, but distinguishing that signal from intrinsic compact structure becomes harder, as was seen in RadioAstron AGN results (M. D. Johnson et al. 2016; S. V. Pilipenko et al. 2018).

4. SUMMARY

TXS 2005+403 is a bright (~ 2 Jy) blazar viewed through the Cygnus region, where Galactic scattering is particularly strong. We detect a long-baseline signal in its VLBI observations that cannot be explained by the diffractive scatter-broadened profile or by intrinsic source structure. We identify this signal as refractive substructure produced by turbulence in the intervening plasma, making TXS 2005+403 the first AGN in which refractive scattering has been directly detected

with ground-based VLBI. This signal is detected from 1.4 to 5 GHz and remains stable across nearly a decade, with amplitudes consistent with theoretical expectations. This consistency indicates a persistently strong scattering screen with stable properties along this line of sight.

These findings establish TXS 2005+403 as an exceptional laboratory for studying Galactic turbulence and scattering physics. The source combines several crucial properties: (i) high flux density (~ 2 Jy), enabling detections with routine VLBI; (ii) compact intrinsic structure on mas and sub-mas scales, necessary for scattering to dominate the observed morphology; (iii) structural stability on timescales of months, unlike Sagittarius A*, where intrinsic variability complicates interpretation; and (iv) strong scattering due to its location behind the turbulent Cygnus region. This detection suggests that similar AGNs in other strongly scattering regions could be identified, enabling systematic studies of Galactic turbulence and magnetic field structure across the sky. Improved understanding of scattering properties from sources like TXS 2005+403 would directly inform efforts to mitigate scattering artifacts in Event Horizon Telescope images of the black hole in the center of the Milky Way, where scattering limits image fidelity, and would help interpret propagation effects in fast radio bursts.

Dedicated VLBI observations with higher sensitivity and more uniform uv coverage can move this result from detection to parameter inference. They will enable direct tests of turbulence models by jointly constraining the inner scale, anisotropy, and magnetic field-aligned structure in the scattering plasma. Multi-epoch time-domain measurements can quantify refractive modulation amplitudes and characteristic variability timescales, constraining the kinematics and evolution of the Cygnus scattering screen along this line of sight. We have initiated VLBA project BP276 with multi-epoch, multi-frequency observations in 2025–2026 to pursue these

goals. Together with the future identification of analogous sources behind strongly scattering Galactic regions, such observations are establishing AGNs as a systematic probe of interstellar turbulence.

ACKNOWLEDGMENTS

We thank Aditya Tamar, Michael Johnson, and Ramesh Narayan for useful comments on the manuscript. AVP is a postdoctoral fellow at the Black Hole Initiative, which is funded by grants from the John Templeton Foundation (grants 60477, 61479, 62286) and the Gordon and Betty Moore Foundation (grant GBMF-8273). ABP was supported by the Russian Science Foundation grant 25-22-00152. YYK was supported by the MuSES project, which has received funding from the European Union (ERC grant agreement No 101142396). The views and opinions expressed in this work are those of the authors and do not necessarily reflect the views of these Foundations. This work made use of results of the Swinburne University of Technology software correlator DiFX (A. T. Deller et al. 2011), developed as part of the Australian Major National Research Facilities Programme and operated under license.

Code to reproduce analysis and figures from this manuscript can be found at <https://github.com/aplavin/txs2005-refractive-substructure>.

Facilities: VLBA

Software: AIPS (E. W. Greisen 2003), Makie.jl (S. Danisch & J. Krumbiegel 2021), Pigeons.jl (N. Surjanovic et al. 2024), ScatteringOptics.jl (<https://github.com/EHTJulia/ScatteringOptics.jl>), ScatteringOpticsExtra.jl (<https://github.com/JuliaAPlavin/ScatteringOpticsExtra.jl>), VLBIData.jl (<https://github.com/JuliaAPlavin/VLBIData.jl>), AccessibleModels.jl (<https://github.com/JuliaAPlavin/AccessibleModels.jl>); a complete list of dependencies is available in the accompanying code repository.

REFERENCES

- Boksenberg, A., Briggs, S. A., Carswell, R. F., Schmidt, M., & Walsh, D. 1976, MNRAS, 177, 43, doi: [10.1093/mnras/177.1.43P](https://doi.org/10.1093/mnras/177.1.43P)
- Danisch, S., & Krumbiegel, J. 2021, Journal of Open Source Software, 6, 3349, doi: [10.21105/joss.03349](https://doi.org/10.21105/joss.03349)
- Deller, A. T., Brisken, W. F., Phillips, C. J., et al. 2011, PASP, 123, 275, doi: [10.1086/658907](https://doi.org/10.1086/658907)
- Duffett-Smith, P. J., & Readhead, A. C. S. 1976, MNRAS, 174, 7, doi: [10.1093/mnras/174.1.7](https://doi.org/10.1093/mnras/174.1.7)
- Greisen, E. W. 2003, in Astrophysics and Space Science Library, Vol. 285, Information Handling in Astronomy - Historical Vistas, ed. A. Heck, 109, doi: [10.1007/0-306-48080-8_7](https://doi.org/10.1007/0-306-48080-8_7)
- Gwinn, C. R., Kovalev, Y. Y., Johnson, M. D., & Soglasnov, V. A. 2014, ApJL, 794, L14, doi: [10.1088/2041-8205/794/1/L14](https://doi.org/10.1088/2041-8205/794/1/L14)
- Gwinn, C. R., Popov, M. V., Bartel, N., et al. 2016, ApJ, 822, 96, doi: [10.3847/0004-637X/822/2/96](https://doi.org/10.3847/0004-637X/822/2/96)

- Issaoun, S., Johnson, M. D., Blackburn, L., et al. 2019, *ApJ*, 871, 30, doi: [10.3847/1538-4357/aaf732](https://doi.org/10.3847/1538-4357/aaf732)
- Johnson, M. D. 2016, *ApJ*, 833, 74, doi: [10.3847/1538-4357/833/1/74](https://doi.org/10.3847/1538-4357/833/1/74)
- Johnson, M. D., & Gwinn, C. R. 2015, *ApJ*, 805, 180, doi: [10.1088/0004-637X/805/2/180](https://doi.org/10.1088/0004-637X/805/2/180)
- Johnson, M. D., Kovalev, Y. Y., Lisakov, M. M., et al. 2021, *ApJL*, 922, L28, doi: [10.3847/2041-8213/ac3917](https://doi.org/10.3847/2041-8213/ac3917)
- Johnson, M. D., & Narayan, R. 2016, *ApJ*, 826, 170, doi: [10.3847/0004-637X/826/2/170](https://doi.org/10.3847/0004-637X/826/2/170)
- Johnson, M. D., Kovalev, Y. Y., Gwinn, C. R., et al. 2016, *ApJL*, 820, L10, doi: [10.3847/2041-8205/820/1/L10](https://doi.org/10.3847/2041-8205/820/1/L10)
- Johnson, M. D., Narayan, R., Psaltis, D., et al. 2018, *ApJ*, 865, 104, doi: [10.3847/1538-4357/aadcff](https://doi.org/10.3847/1538-4357/aadcff)
- Koryukova, T. A., Pushkarev, A. B., Kiehlmann, S., & Readhead, A. C. S. 2023, *MNRAS*, 526, 5932, doi: [10.1093/mnras/stad3052](https://doi.org/10.1093/mnras/stad3052)
- Koryukova, T. A., Pushkarev, A. B., Plavin, A. V., & Kovalev, Y. Y. 2022, *MNRAS*, 515, 1736, doi: [10.1093/mnras/stac1898](https://doi.org/10.1093/mnras/stac1898)
- Koryukova, T. A., Trushkin, S. A., Pashchenko, I. N., & Pushkarev, A. B. 2025, *MNRAS*, 542, 2733, doi: [10.1093/mnras/staf1369](https://doi.org/10.1093/mnras/staf1369)
- Kovalev, Y. Y., Kardashev, N. S., Sokolovsky, K. V., et al. 2020, *Advances in Space Research*, 65, 705, doi: [10.1016/j.asr.2019.08.035](https://doi.org/10.1016/j.asr.2019.08.035)
- Lister, M. L., Homan, D. C., Kellermann, K. I., et al. 2021, *ApJ*, 923, 30, doi: [10.3847/1538-4357/ac230f](https://doi.org/10.3847/1538-4357/ac230f)
- Narayan, R., & Goodman, J. 1989, *MNRAS*, 238, 963, doi: [10.1093/mnras/238.3.963](https://doi.org/10.1093/mnras/238.3.963)
- Petrov, L., Kovalev, Y. Y., Fomalont, E. B., & Gordon, D. 2011, *AJ*, 142, 35, doi: [10.1088/0004-6256/142/2/35](https://doi.org/10.1088/0004-6256/142/2/35)
- Petrov, L. Y., & Kovalev, Y. Y. 2025, *ApJS*, 276, 38, doi: [10.3847/1538-4365/ad8c36](https://doi.org/10.3847/1538-4365/ad8c36)
- Pilipenko, S. V., Kovalev, Y. Y., Andrianov, A. S., et al. 2018, *MNRAS*, 474, 3523, doi: [10.1093/mnras/stx2991](https://doi.org/10.1093/mnras/stx2991)
- Plavin, A. V., Kovalev, Y. Y., & Pushkarev, A. B. 2022, *ApJS*, 260, 4, doi: [10.3847/1538-4365/ac6352](https://doi.org/10.3847/1538-4365/ac6352)
- Popov, M. V., Bartel, N., Burgin, M. S., et al. 2020, *ApJ*, 888, 57, doi: [10.3847/1538-4357/ab5db6](https://doi.org/10.3847/1538-4357/ab5db6)
- Popov, M. V., Bartel, N., Gwinn, C. R., et al. 2017, *MNRAS*, 465, 978, doi: [10.1093/mnras/stw2353](https://doi.org/10.1093/mnras/stw2353)
- Pushkarev, A. B., & Kovalev, Y. Y. 2015, *MNRAS*, 452, 4274, doi: [10.1093/mnras/stv1539](https://doi.org/10.1093/mnras/stv1539)
- Pushkarev, A. B., Kovalev, Y. Y., Lister, M. L., et al. 2013, *A&A*, 555, A80, doi: [10.1051/0004-6361/201321484](https://doi.org/10.1051/0004-6361/201321484)
- Rickett, B. J. 1990, *ARA&A*, 28, 561, doi: [10.1146/annurev.aa.28.090190.003021](https://doi.org/10.1146/annurev.aa.28.090190.003021)
- Rygl, K. L. J., Brunthaler, A., Sanna, A., et al. 2012, *A&A*, 539, A79, doi: [10.1051/0004-6361/201118211](https://doi.org/10.1051/0004-6361/201118211)
- Savolainen, T., Giovannini, G., Kovalev, Y. Y., et al. 2023, *A&A*, 676, A114, doi: [10.1051/0004-6361/202142594](https://doi.org/10.1051/0004-6361/202142594)
- Surjanovic, N., Biron-Lattes, M., Tiede, P., et al. 2024, *Proceedings of the JuliaCon Conferences*, 6, 139, doi: [10.21105/jcon.00139](https://doi.org/10.21105/jcon.00139)